Journal of Materials Chemistry C

ROYAL SOCIETY OF CHEMISTRY

PAPER

View Article Online
View Journal | View Issue

Cite this: J. Mater. Chem. C, 2024, 12, 4648

Subphthalocyanine semiconducting cocrystals with efficient super-exchange coupling†

Lingyan Sun,[a] Yuan Guo,*[bc] Dan He,[d] Barun Dhara,[e] Fei Huang,[a] Yuanping Yi,[c] Daigo Miyajima*[f] and Cheng Zhang *[a]

Received 23rd January 2024,
Accepted 27th February 2024

DOI: 10.1039/d4tc00333k

rsc.li/materials-c

Organic cocrystals have attracted widespread research attention due to their unique properties. However, the development of crystal engineering is relatively slow because of the difficulty in designing the molecular structures and controlling the intermolecular interactions. Here, we report a subphthalocyanine (SubPc) cocrystal (**SubPc-12H-12F**) through preciously regulating hydrogen bonds and donor–acceptor interactions. The cocrystal forms a perfect one-dimensional columnar assembly and shows an almost identical packing mode with a one-component single crystal **SubPc-6F(β)**, which provides an ideal example to study the super-exchange coupling in cocrystals. The **SubPc-12H-12F** cocrystal exhibits ambipolar transport properties with an improved hole mobility of 0.019 $cm^2 V^{-1} s^{-1}$ by two orders of magnitude compared with **SubPc-6F(β)**. The cocrystals of **SubPc-12H-12F** exhibit the highest mobilities ever reported among SubPc derivatives and surpass the order of 10^{-2} $cm^2 V^{-1} s^{-1}$ for the first time. Theoretical calculations indicated that the super-exchange coupling in cocrystals can both increase the charge carrier mobility and expand the charge transport channels, which holds the potential to further predictions for high-performance cocrystals.

Introduction

With the rapid advances in crystal engineering and supramolecular chemistry, organic cocrystals exhibit significant potential in materials science, such as room-temperature phosphorescence,[1–4] charge transport properties,[5–7] ferroelectricity,[8–13] bulk photovoltaic effects,[14] *etc.* Compared with chemical synthesis to construct high-performance materials, the development of crystal engineering still lags far behind because of the difficulty in designing the molecular structures, controlling the intermolecular interactions, and matching the solubilities.[15,16] In contrast with planar-shape semiconductors, bowl-shaped conjugated molecules with concave–convex complementary structures are more likely to form columnar packing, which results in a limited π-surface overlap and inferior charge transport.[17–20] Recently, organic cocrystalline semiconductors with two or more different components in a stoichiometric ratio have unique ambipolar charge transport characteristics and have revealed the structure–property relationships at molecular levels, which emerges as promising research

[a] *Key Laboratory of Green Chemistry and Technology of Ministry of Education, College of Chemistry, Sichuan University, Chengdu 610064, P. R. China. E-mail: cheng.zhang@scu.edu.cn*
[b] *School of Light Industry and Engineering, Qilu University of Technology (Shandong Academy of Sciences), Jinan 250353, P. R. China. E-mail: yguo@qlu.edu.cn*
[c] *Beijing National Laboratory for Molecular Sciences, CAS Key Laboratory of Organic Solids, Institute of Chemistry, Chinese Academy of Sciences, Beijing 100190, P. R. China*
[d] *College of Chemistry and Chemical Engineering, Central South University, Changsha 410083, P. R. China*
[e] *RIKEN Center for Emergent Matter Science, 2-1 Hirosawa, Wako, Saitama 351-0198, Japan*
[f] *School of Science and Engineering, The Chinese University of Hong Kong, Shenzhen 518172, P. R. China. E-mail: dmiyajima@cuhk.edu.cn*

† Electronic supplementary information (ESI) available. CCDC 2288075. For ESI and crystallographic data in CIF or other electronic format see DOI: https://doi.org/10.1039/d4tc00333k

Cheng Zhang

Cheng Zhang received his BSc and PhD degrees in Chemistry from the Wuhan University in 2012 and Institute of Chemistry, Chinese Academy of Sciences (ICCAS) in 2017. Dr Zhang then worked at CEMS, RIKEN in Japan as a Special Postdoctoral Researcher supervised by Prof. Takuzo Aida and Prof. Daigo Miyajima. After this, he worked as a PI at the College of Chemistry, Sichuan University from 2021. His research interest is now focused on optoelectronic device applications based on semiconductor materials with spontaneous polarization.

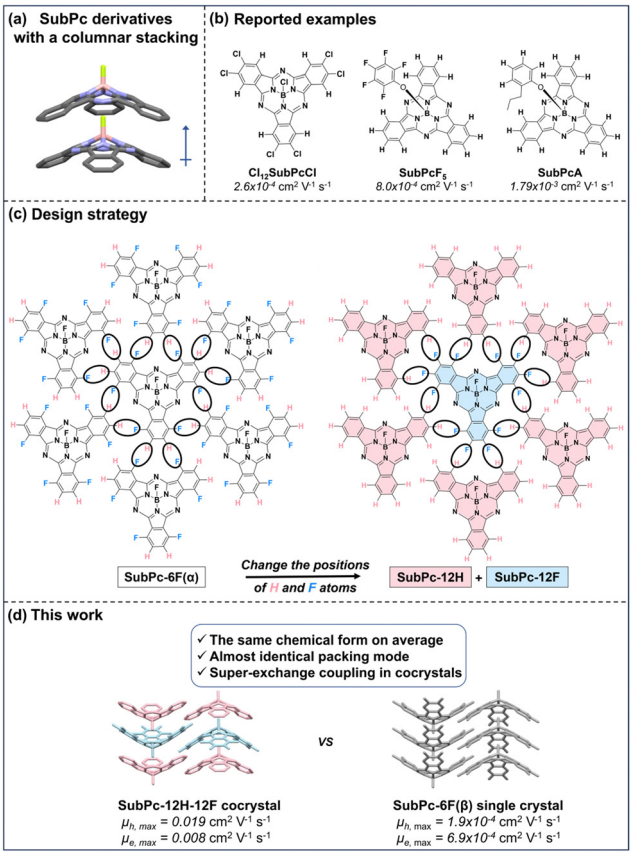

Fig. 1 (a) Columnar stacking mode and (b) reported mobilities of SubPc derivatives. Schematic illustration of (c) the design strategy to build the **SubPc-12H-12F** cocrystal with (d) the mobilities compared with the **SubPc-6F(β)** single crystal with almost identical packing.

interest in materials science.[21–24] However, the reported charge carrier mobilities of bowl-shaped cocrystals are still at the order of 10^{-1} cm^2 V^{-1} s^{-1} magnitude.[25–27] Subphthalocyanines (SubPcs) are a class of conjugate molecules with a bowl-shaped structure, which are composed of a central boron atom, three isoindole units and an axial ligand.[28–30] The unique bowl-shaped structure of SubPcs results in a large dipole moment in the axial direction and are applied in organic solar cells,[31–34] organic photodetectors,[30,35] nonlinear optics,[28,36] singlet fission,[37–39] *etc.*, recently. By using the fluoride atom as the axial ligand, Torres *et al.*[40,41] reported the perfect one-dimensional assemblies of SubPcs (Fig. 1a). These one-dimensional columns amplify the dipole moment and are convenient for charge separation and transport. However, SubPcs were rarely applied in the field of charge transport and the mobilities of SubPcs were only at 10^{-3} cm^2 V^{-1} s^{-1} level as the highest (Fig. 1b) because of the limited π–π interactions.[42–44]

In this study, we chose SubPc as a model compound to construct cocrystals through precisely modulating the intermolecular interactions. This cocrystal exhibits ambipolar charge transport properties in organic field-effect transistor (OFET) devices. To our surprise, the hole mobilities of cocrystals improve two orders of magnitude to the SubPc single crystals with almost identical packing and surpass the order of 10^{-2} cm^2 V^{-1} s^{-1}, while 8.5 times for the electron mobilities. Furthermore, theoretical calculations unveiled the importance of the super-exchange effect[45–47] in cocrystals for the remarkable enhancement in carrier mobilities. We believe that this design strategy as well as the super-exchange effect evaluation will open up new avenues for the study of charge transport in organic cocrystals and the design of high-performance bowl-shaped semiconductors.

Results and discussion

Previously, we reported a design strategy to build polar SubPc crystals with a trigonal lattice through hydrogen bond modulation, for instance, **SubPc-6F(α)** with half and half fluoride and hydrogen atoms at isoindole units.[48] If we separate all fluoride and hydrogen atoms of **SubPc-6F(α)** into two different molecules, **SubPc-12F** and **SubPc-12H** (Fig. 1c), we assume that the same molecular packing can also be depicted because the same hydrogen bond networks are expected. To the best of our knowledge, the SubPc-SubPc cocrystals are unprecedented.[49–51]

We synthesized **SubPc-12H** and **SubPc-12F** according to the reported literature studies.[40,52] After numerous attempts, **SubPc-12H-12F** cocrystals were finally obtained with a 1 : 1 mole ratio of **SubPc-12H** and **SubPc-12F** both from a solvent diffusion method (mixture of $CHCl_3$ and ethanol) and a physical vapor transport (PVT) process (Fig. S11 and Table S4, ESI†). Especially, in the PVT process, **SubPc-12H** and **SubPc-12F** were placed at each side of the glass tube and the **SubPc-12H-12F** cocrystals were gradually formed in the middle of the tube by cosublimation. The schematic diagram and the sublimation conditions of the PVT process are shown in Fig. S11a and Table S4 (ESI†). After X-ray structural analysis, we surprisingly found that the stacking modes are quite similar to the single crystals of **SubPc-6F(β)** we reported previously.[48] The details will be discussed below.

As shown in Fig. 2, both **SubPc-12H-12F** cocrystals and **SubPc-6F(β)** single crystals assemble in one-dimensional columns with antiparallel orientations. The two components in **SubPc-12H-12F** cocrystals perform the ABAB stacking mode in columns. These crystals are monoclinic with a $P2_1/m$ space group. As summarized in Table 1, **SubPc-12H-12F** cocrystals have similar cell parameters (b, c, α, β, and γ) and B–B distance and π–π distance to **SubPc-6F(β)**. The double a-axis value of **SubPc-12H-12F** is attributed to the two components in cocrystals. The intermolecular interactions of **SubPc-12H-12F** and **SubPc-6F(β)** were evaluated by Hirshfeld surface analysis[53] (Fig. S5 and S6, ESI†). The profiles of intermolecular interactions in **SubPc-12H-12F** and **SubPc-6F(β)** are almost the same as expected. Besides, due to the electrostatic force coming from the donor and acceptor in columns, the bowl depths of **SubPc-12H** and **SubPc-12F** in **SubPc-12H-12F** cocrystals are 2.79 and 2.89 Å, deeper than the ones in **SubPc-12H** (2.48 Å) and **SubPc-12F** (2.71 Å) single crystals, respectively (Fig. S3, S4 and Table S1, ESI†). At the same time, the larger density of the **SubPc-12H-12F** cocrystal indicates closer stackings compared with that of the **SubPc-6F(β)**, which may be more efficient for charge

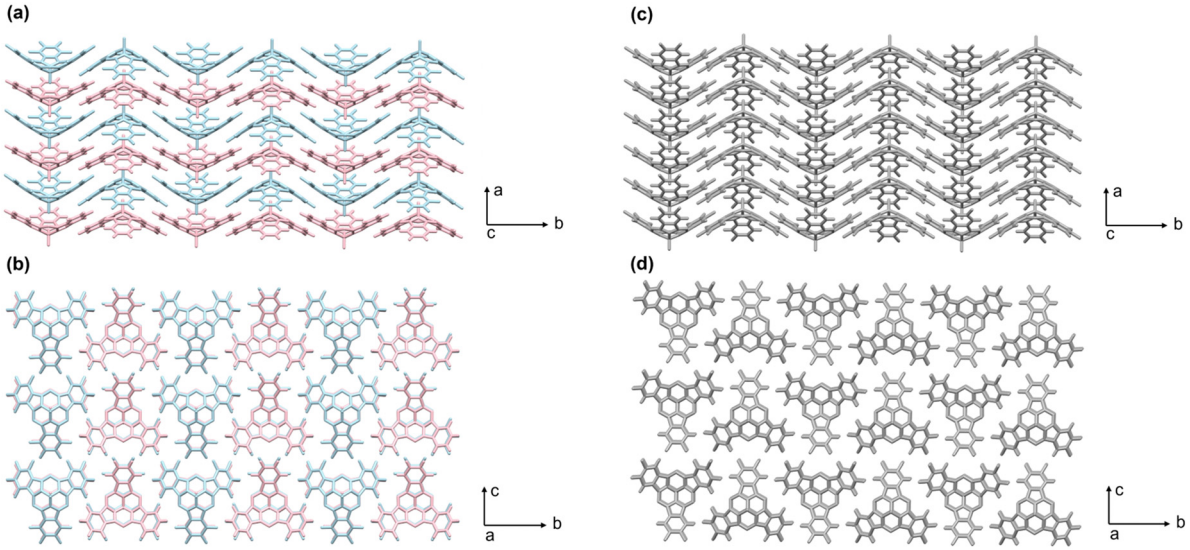

Fig. 2 X-ray crystal structures of (a) and (c) side views and (b) and (d) top views of (a) and (b) **SubPc-12H-12F** and (c) and (d) **SubPc-6F(β)**.

Table 1 Crystallographic data of **SubPc-12H-12F** and **SubPc-6F(β)**

Crystals	**SubPc-12H-12F**[a]	**SubPc-6F(β)**[b]
Crystal system	Monoclinic	Monoclinic
Crystal symmetry	C_{2h}	C_{2h}
Space group	$P2_1/m$	$P2_1/m$
a [Å]	8.6916(2)	4.3804(10)
b [Å]	19.7951(5)	19.3454(5)
c [Å]	11.5578(3)	12.1264(4)
α [°]	90	90
β [°]	95.196(7)	99.012(3)
γ [°]	90	90
V [Å^3]	1980.36(9)	1014.91(5)
Density [g cm^{-3}]	1.751	1.709
R [%]	4.57	4.34
R_w [%]	11.12	11.55
B–B distance [Å]	4.35	4.38
π–π distance[c] [Å]	3.50	3.50

[a] CCDC 2288075. [b] From ref. 12. [c] The distances were the shortest among the three SubPc arms.

transport. As a result, **SubPc-12H-12F** and **SubPc-6F(β)** have the same chemical form on average and almost identical packing modes, which provide an ideal instance to investigate the super-exchange couplings in cocrystals and compare the charge transport properties in cocrystals and mono-component single crystals.

The UV/Vis absorption spectra, electrochemical cyclic voltammograms (CVs) and ultraviolet photoelectron spectra (UPS) were recorded to explore the photophysical and electrochemical properties of crystals. Samples for UPS measurements were prepared by PVT methods onto ITO substrates. The data of **SubPc-12H-12F** cocrystals, **SubPc-6F(β)**, **SubPc-12H** and **SubPc-12F** single crystals are summarized in Fig. 3 and Table 2. All the crystals exhibit broad absorption in the visible region. The maximum absorption values of **SubPc-12H-12F**, **SubPc-6F(β)**, **SubPc-12H** and **SubPc-12F** crystals are 612, 595, 639, and 606 nm, respectively. With the decreased number of electron-withdrawing F atoms, the highest occupied molecular orbital (HOMO) and the lowest unoccupied molecular orbital (LUMO) energy levels of **SubPc-12F**, **SubPc-6F(β)** and **SubPc-12H** estimated from CV in dilute CH_2Cl_2 (Fig. S8–S10 and Table S3, ESI†) are increased gradually from −5.71 to −5.32 eV and −3.85 to −3.33 eV, respectively. The tendency evaluated from the density functional theory (DFT) calculation (Fig. 3c) agrees well with the experimental data. Meanwhile, we also calculated the HOMO energy levels of these four crystals from UPS spectra with almost identical edge shapes. The increments of the HOMO energy levels of **SubPc-12F** (−6.06 eV), **SubPc-6F(β)**

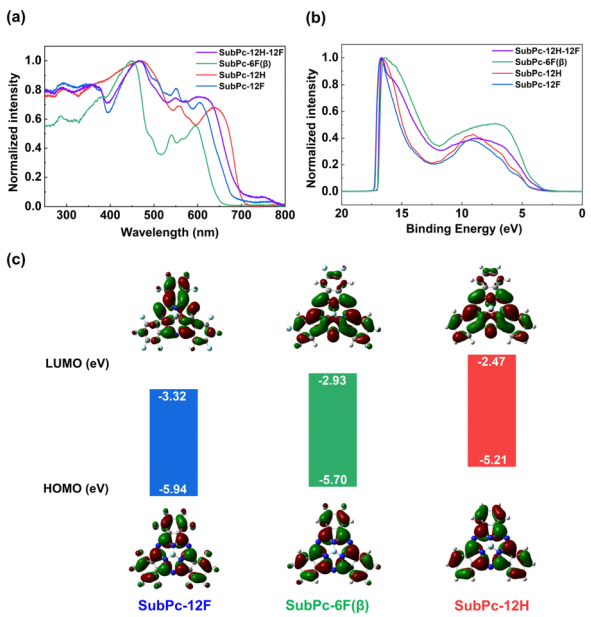

Fig. 3 (a) UV-vis absorption spectra and (b) UPS results of **SubPc-12H-12F**, **SubPc-6F(β)**, **SubPc-12H** and **SubPc-12F** in crystalline states. (c) Calculated molecular orbital diagrams and energy levels of **SubPc-12F**, **SubPc-6F(β)**, and **SubPc-12H** in a vacuum.

Table 2 Photophysical and electrochemical properties of **SubPc-12H-12F**, **SubPc-6F(β)**, **SubPc-12H** and **SubPc-12F**

Materials	λ_{max} [a] [nm]	E_g [b] [eV]	HOMO [c] [eV]
SubPc-12H-12F	612	1.77	−5.86
SubPc-6F(β)	595	1.92	−5.81
SubPc-12H	639	1.78	−5.09
SubPc-12F	606	1.83	−6.06

[a] Absorption maxima of crystals. [b] The optical bandgaps were calculated according to $E_g = 1240/\lambda_{onset}$, where λ_{onset} is the onset value of the absorption spectrum in the long wavelength region. [c] Estimated from the empirical equation HOMO = WF + E_b (eV), where WF is the *d*-value between 21.22 and the onset value of the high binding energy, and E_b is the onset value of the low binding energy.

(−5.81 eV), and **SubPc-12H** (−5.09 eV) crystals are consistent with those calculated from CV measurements. Importantly, the HOMO energy level of **SubPc-12H-12F** (−5.86 eV) cocrystals is similar to that of **SubPc-6F(β)** and in between with **SubPc-12H** and **SubPc-12F**, which demonstrates that the energy levels of cocrystals can also be fine-tuned like single crystals.[54–56]

As shown in Fig. 4a and b, the needle-like purple-red crystals of **SubPc-12H-12F** and **SubPc-6F(β)** could be obtained regardless of the solvent diffusion or the PVT method. To figure out the molecular orientations of **SubPc-12H-12F** and **SubPc-6F(β)**, X-ray diffraction (XRD, Fig. 4c and d) and selected-area electron diffraction (SAED, Fig. 4e and f) were performed. The XRD patterns exhibit sharp diffraction peaks at 7.91° (*d* = 11.29 Å) and 9.12° (*d* = 9.69 Å) in **SubPc-12H-12F** and 7.33° (*d* = 12.01 Å) and 8.73° (*d* = 10.03 Å) in **SubPc-6F(β)**, which are consistent with the simulated patterns, indicating that the planes (001), (020) and (001), (011) are dominant when **SubPc-12H-12F** and **SubPc-6F(β)** evaporate on substrates, respectively. After simulating the growth morphologies (the inset of Fig. 4e and f) based on the Bravais–Friedel–Donnay–Harker (BFDH) method using the Mercury program,[57] we found that they are in agreement with the crystal shapes in optical images and the dominant crystal planes in XRD results. All the SAED patterns by transmission electron microscopy can also be indexed from the XRD analysis. As a result, the columns are arranged along the long axis (*a*-axis) in both **SubPc-12H-12F** cocrystals and **SubPc-6F(β)** single crystals.

We fabricated the single crystal OFETs with a bottom-gate top-contact (BGTC) configuration and checked the performance along the long axis of crystals. The **SubPc-12H-12F** cocrystals and **SubPc-6F(β)** single crystals were sublimated onto octadecyltrichlorosilane (OTS)-modified SiO_2 (300 nm)/Si substrates, and then 60 nm gold was evaporated as the source and drain electrodes (Fig. S12 and S13, ESI†). The representative transfer and output curves of devices based on **SubPc-12H-12F** and **SubPc-6F(β)** are shown in Fig. 5a, b and Fig. S14 (ESI†), respectively, and the device characteristics are summarized in Table 3, demonstrating typical features of ambipolar transporting organic semiconductors. The mobilities are extracted from at least 10 devices and the maximum values and the statistical results are illustrated in Fig. 5c and d. For **SubPc-6F(β)**, the average hole and electron mobilities are 1.1 × 10^{-4} and 6.4 × 10^{-4} $cm^2 V^{-1} s^{-1}$ with maximum values of 1.9 × 10^{-4} and 9.1 × 10^{-4} $cm^2 V^{-1} s^{-1}$, respectively. Whereas for **SubPc-12H-12F**, the average hole and electron mobilities are increased to 0.012 and 0.003 $cm^2 V^{-1} s^{-1}$ with the maximum values reaching 0.019 and 0.008 $cm^2 V^{-1} s^{-1}$, respectively. Unexpectedly, the maximum mobilities of **SubPc-12H-12F** for holes and electrons are 100 and 8.5 times higher than those of **SubPc-6F(β)**, despite sharing the same chemical form on average and exhibiting almost identical packing arrangements. As far as we are aware, the **SubPc-12H-12F** cocrystals exhibit the highest mobilities up

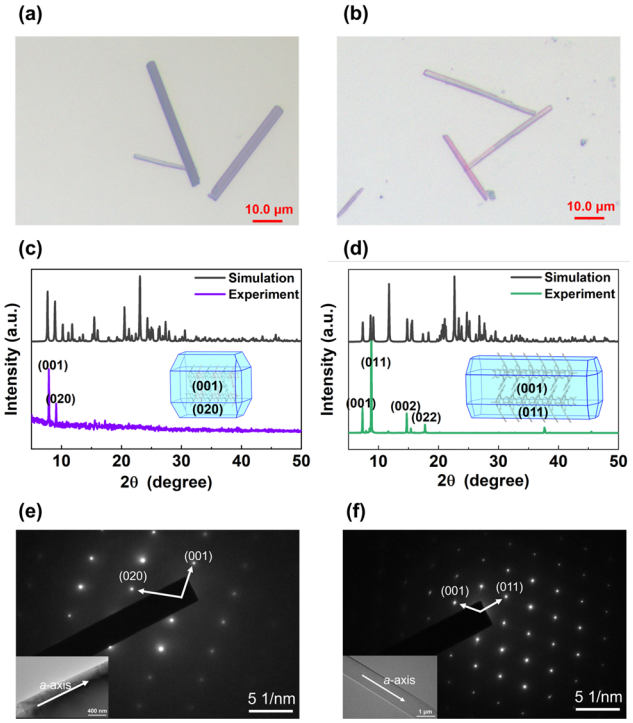

Fig. 4 (a) and (b) Optical images, (c) and (d) XRD patterns and (e) and (f) corresponding SAED patterns of (a), (c) and (e) **SubPc-12H-12F** and (b), (d) and (f) **SubPc-6F(β)**. The inserted images in (c) and (d) were the calculated morphologies and (e) and (f) were the TEM images of **SubPc-12H-12F** and **SubPc-6F(β)**.

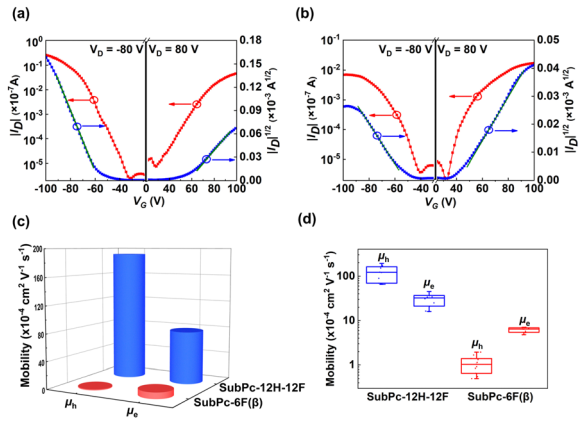

Fig. 5 The representative transfer curves of (a) **SubPc-12H-12F** and (b) **SubPc-6F(β)** in OFET devices. (c) The maximum and (d) the statistical mobilities of **SubPc-12H-12F** and **SubPc-6F(β)**.

Table 3 OFET device performances of **SubPc-12H-12F** and **SubPc-6F(β)**[a]

	Hole mobility			Electron mobility		
Materials	μ_h [$\times 10^{-4}$ cm^2 V^{-1} s^{-1}]	V_{th} [V]	$I_{on/off}$	μ_e [$\times 10^{-4}$ cm^2 V^{-1} s^{-1}]	V_{th} [V]	$I_{on/off}$
SubPc-12H-12F	191.0 (122.0)	−25 (−51)	10^5 (10^4)	77.5 (30.4)	20 (43)	10^4 (10^3)
SubPc-6F(β)	1.9 (1.1)	−26 (−44)	10^4 (10^3)	9.1 (6.4)	24 (35)	10^4 (10^3)

[a] Averaged from 10 devices. The devices were tested under a N_2 atmosphere.

to date in SubPc derivatives and surpass the order of 10^{-2} cm^2 V^{-1} s^{-1} for the first time.

To delve into why **SubPc-12H-12F** cocrystals exhibit enhanced mobilities than **SubPc-6F(β)** single crystals, we further conducted theoretical calculations. First, the transfer integrals and reorganization energies were estimated based on the crystal data (Fig. S15 and Table S5, ESI†). The reorganization energies of both crystals are similar for holes (146 meV for **SubPc-12H-12F** and 120 meV for **SubPc-6F(β)**) and electrons (310 meV for **SubPc-12H-12F** and 300 meV for **SubPc-6F(β)**), respectively. The dimer of **SubPc-6F(β)** in a column has much bigger transfer integral (t_1) values than that of **SubPc-12H-12F** for both hole and electron transports. Meanwhile, the little t_2 values of dimers in adjacent columns indicate only one dimensional (1D) channel for charge transport in both **SubPc-12H-12F** cocrystals and **SubPc-6F(β)** single crystals. The anisotropy mobility evaluation of **SubPc-6F(β)** (Fig. 6e and f) shows the same tendency, which could only transport along *a*-axis.

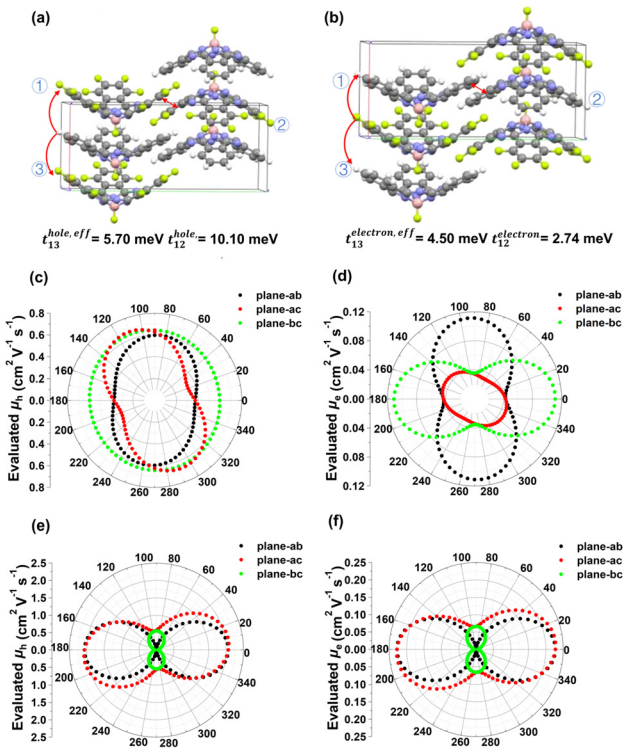

Fig. 6 (a) Hole and (b) electron couplings of **SubPc-12H-12F**. The anisotropy of (c) and (e) hole and (d) and (f) electron mobilities in different planes of the (c) and (d) **SubPc-12H-12F** and (e) and (f) **SubPc-6F(β)** crystals without considering the site energy difference.

Although the transfer integrals and reorganization energy calculations suggested that **SubPc-6F(β)** should exhibit superior device performance, the experimental results yielded contradictory outcomes. Next, we examined the super-exchange couplings, which are derived in a D–A–D or A–D–A triad system in organic D–A cocrystals and copolymers.[45–47] Because of the ambipolar transport characteristics of **SubPc-12H-12F**, we assumed that holes could transport from molecule 1 to 3, resulting in a super-exchange coupling value of 5.70 meV (Fig. 6a). Notably, multiple super-exchange coupling triads exist in this cocrystal. When considering only this triad for evaluating carrier mobility, we observed an increase in hole mobility from 0.53 to 0.93 cm^2 V^{-1} s^{-1}, surpassing 0.89 cm^2 V^{-1} s^{-1} of **SubPc-6F(β)** estimated through the semi-classical Marcus (Table S6, ESI†). Simultaneously (Fig. 6b), the electron mobility can be improved from 0.059 to 0.086 cm^2 V^{-1} s^{-1}, exceeding 0.076 cm^2 V^{-1} s^{-1} of **SubPc-6F(β)**. Moreover, in **SubPc-12H-12F** cocrystals, the channels for charge transport extend from 1D to 2D for electrons (Fig. 6d) and even 3D for holes (Fig. 6c) due to super-exchange coupling, resulting in higher hole mobilities than those of electrons. These calculation results demonstrate that the super-exchange coupling plays an important role in charge transport in cocrystals. The presence of multiple channels in **SubPc-12H-12F** cocrystals facilitates the smoother transport of charge carriers, as they can switch to an alternative channel in the case of defects. Conversely, charge carriers tend to be trapped in **SubPc-6F(β)**. Consequently, cocrystals have the potential to obtain higher mobilities compared to single crystals with analogous packings.

Conclusions

In summary, we have successfully obtained **SubPc-12H-12F** cocrystals through precious molecular design. Notably, **SubPc-12H-12F** demonstrates ambipolar transport characteristics, exhibiting hole and electron mobilities up to 0.019 and 0.008 cm^2 V^{-1} s^{-1}, respectively. These values are significantly elevated compared to **SubPc-6F(β)**, displaying an increase of 100 and 8.5 times, respectively, despite their nearly identical packing modes. This marks the first instance of enhancing SubPcs' mobilities to the order of 10^{-2} cm^2 V^{-1} s^{-1} through crystal engineering. Moreover, the super-exchange coupling in cocrystals not only enhances carrier mobility but also broadens the charge transport channels. This observation is in excellent agreement with the experimental findings. Thus, our approach, combining theoretical calculations with strategic design, holds the potential to further predictions for high-performance

bowl-shaped cocrystals. We trust that this contribution will advance the field of organic cocrystal materials.

Conflicts of interest

The authors declare no competing interests.

Acknowledgements

We acknowledge the financial support from the National Natural Science Foundation of China (22205150, 22203049, and 52272056) and the Fundamental Research Funds for the Central Universities. We also thank the help of Yunfei Tian from the Analytical & Testing Center of Sichuan University and Feng Yang from the Comprehensive Training Platform of the Specialized Laboratory in the College of Chemistry at Sichuan University for the UPS measurement and TEM test, respectively.

References

1 A. Abe, K. Goushi, M. Mamada and C. Adachi, *Adv. Mater.*, 2023, 2211160.
2 L. Ma, Y. Liu, H. Tian and X. Ma, *JACS Au*, 2023, **3**, 1835.
3 T. Zhang, X. Ma, H. Wu, L. Zhu, Y. Zhao and H. Tian, *Angew. Chem., Int. Ed.*, 2020, **59**, 11206.
4 J. Yang, M. Fang and Z. Li, *Acc. Mater. Res.*, 2021, **2**, 644.
5 L. Sun, Y. Wang, F. Yang, X. Zhang and W. Hu, *Adv. Mater.*, 2019, **31**, 1902328.
6 F. Li, L. Zheng, Y. Sun, S. Li, L. Sun, F. Yang, W. Dong, X. Zhang and W. Hu, *Sci. China: Chem.*, 2023, **66**, 266.
7 J. Zhang, J. Tan, Z. Ma, W. Xu, G. Zhao, H. Geng, C. Di, W. Hu, Z. Shuai, K. Singh and D. Zhu, *J. Am. Chem. Soc.*, 2013, **135**, 558.
8 Y. Huang, Z. Wang, Z. Chen and Q. Zhang, *Angew. Chem., Int. Ed.*, 2019, **58**, 9696.
9 A. S. Tayi, A. K. Shveyd, A. C.-H. Sue, J. M. Szarko, B. S. Rolczynski, D. Cao, T. J. Kennedy, A. A. Sarjeant, C. L. Stern, W. F. Paxton, W. Wu, S. K. Dey, A. C. Fahrenbach, J. R. Guest, H. Mohseni, L. X. Chen, K. L. Wang, J. F. Stoddart and S. I. Stupp, *Nature*, 2012, **488**, 485.
10 F. Kagawa, S. Horiuchi, M. Tokunaga, J. Fujioka and Y. Tokura, *Nat. Phys.*, 2010, **6**, 169.
11 R. A. Wiscons, N. R. Goud, J. T. Damron and A. J. Matzger, *Angew. Chem., Int. Ed.*, 2018, **57**, 9044.
12 S. Horiuchi, K. Kobayashi, R. Kumai, N. Minami, F. Kagawa and Y. Tokura, *Nat. Commun.*, 2015, **6**, 7469.
13 E. Collet, M.-H. Lemee-Cailleau, M. B.-L. Cointe, H. Cailleau, M. Wulff, T. Luty, S.-Y. Koshihara, M. Meyer, L. Toupet, P. Rabiller and S. Techert, *Science*, 2003, **300**, 612.
14 M. Nakamura, S. Horiuchi, F. Kagawa, N. Ogawa, T. Kurumaji, Y. Tokura and M. Kawasaki, *Nat. Commun.*, 2017, **8**, 281.
15 J. Zhang, W. Xu, P. Sheng, G. Zhao and D. Zhu, *Acc. Chem. Res.*, 2017, **50**, 1654.
16 L. Sun, W. Zhu, X. Zhang, L. Li, H. Dong and W. Hu, *J. Am. Chem. Soc.*, 2021, **143**, 19243.
17 B. M. Schmidt, S. Seki, B. Topolinski, K. Ohkubo, S. Fukuzumi, H. Sakurai and D. Lentz, *Angew. Chem., Int. Ed.*, 2012, **51**, 11385.
18 K. Shi, T. Lei, X.-Y. Wang, J.-Y. Wang and J. Pei, *Chem. Sci.*, 2014, **5**, 1041.
19 B. Fu, X. Hou, C. Wang, Y. Wang, X. Zhang, R. Li, X. Shao and W. Hu, *Chem. Commun.*, 2017, **53**, 11407.
20 T. Amaya, S. Seki, T. Moriuchi, K. Nakamoto, T. Nakata, H. Sakane, A. Saeki, S. Tagawa and T. Hirao, *J. Am. Chem. Soc.*, 2009, **131**, 408.
21 Y. Qin, C. Cheng, H. Geng, C. Wang, W. Hu, W. Xu, Z. Shuai and D. Zhu, *Phys. Chem. Chem. Phys.*, 2016, **18**, 14094.
22 S. Li, L. Zheng, Y. Chan, B. Li, Y. Sun, L. Sun, C. Zhen, X. Zhang and W. Hu, *J. Mater. Chem. C*, 2022, **10**, 9596.
23 S. K. Park, S. Varghese, J. H. Kim, S. J. Yoon, O. K. Kwon, B. K. An, J. Gierschner and S. Y. Park, *J. Am. Chem. Soc.*, 2013, **135**, 4757.
24 J. Guo, Y. Zeng, Y. Zhen, H. Geng, Z. Wang, Y. Yi, H. Dong and W. Hu, *Angew. Chem., Int. Ed.*, 2022, **61**, e202202336.
25 Y. Wang, Y. Li, W. Zhu, J. Liu, X. Zhang, R. Li, Y. Zhen, H. Dong and W. Hu, *Nanoscale*, 2016, **8**, 14920.
26 R.-Q. Lu, S. Wu, Y.-H. Bao, L.-L. Yang, H. Qu, M. Saha, X.-Y. Wang, Y.-Z. Zhuo, B. Xu, J. Pei, H. Zhang, W. Weng and X.-Y. Cao, *Chem. – Asian J.*, 2018, **13**, 2934.
27 G. Gao, M. Chen, J. Roberts, M. Feng, C. Xiao, G. Zhang, S. Parkin, C. Risko and L. Zhang, *J. Am. Chem. Soc.*, 2020, **142**, 2460.
28 C. G. Claessens, D. Gonzalez-Rodríguez, M. SalomeRodriguez-Morgade, A. Medina and T. Torres, *Chem. Rev.*, 2014, **114**, 2192.
29 S. Shimizu, *Chem. Rev.*, 2017, **117**, 2730.
30 G. Lavarda, J. Labella, M. V. Martinez-Diaz, M. S. Rodriguez-Morgade, A. Osuka and T. Torres, *Chem. Soc. Rev.*, 2022, **51**, 9482.
31 H. T. Chandran, T.-W. Ng, Y. Foo, H.-W. Li, J. Qing, X.-K. Liu, C.-Y. Chan, F.-L. Wong, J. A. Zapien, S.-W. Tsang, M.-F. Lo and C.-S. Lee, *Adv. Mater.*, 2017, **29**, 1606909.
32 K. L. Mutolo, E. I. Mayo, B. P. Rand, S. R. Forrest and M. E. Thompson, *J. Am. Chem. Soc.*, 2006, **128**, 8108.
33 K. Cnops, G. Zango, J. Genoe, P. Heremans, M. V. Martinez-Diaz, T. Torres and D. Cheyns, *J. Am. Chem. Soc.*, 2015, **137**, 8991.
34 S. M. Menke, W. A. Luhman and R. J. Holmes, *Nat. Mater.*, 2013, **12**, 152.
35 C. Zhang, K. Nakano, M. Nakamura, F. Araoka, K. Tajima and D. Miyajima, *J. Am. Chem. Soc.*, 2020, **142**, 3326.
36 G. Torre, P. Vazquez, F. Agullo-Lopez and T. Torres, Role of Structural Factors in the Nonlinear Optical Properties of Phthalocyanines and Related Compounds, *Chem. Rev.*, 2004, **104**, 3723.
37 G. Lavarda, J. Zirzlmeier, M. Gruber, P. R. Rami, R. R. Tykwinski, T. Torres and D. M. Guldi, *Angew. Chem., Int. Ed.*, 2018, **57**, 16291.
38 D. Guzman, I. Papadopoulos, G. Lavarda, P. R. Rami, R. R. Tykwinski, M. S. Rodriguez-Morgade, D. M. Guldi and T. Torres, *Angew. Chem., Int. Ed.*, 2021, **60**, 1474.

39 J. Zirzlmeier, G. Lavarda, H. Gotfredsen, I. Papadopoulos, L. Chen, T. Clark, R. R. Tykwinski, T. Torres and D. M. Guldi, *Nanoscale*, 2020, **12**, 23061.
40 E. Bukuroshi, J. Vestfrid, Z. Gross and T. P. Bender, *New J. Chem.*, 2019, **43**, 16730.
41 M. S. Rodrguez-Morgade, C. G. Claessens, A. Medina, D. Gonzlez-Rodrguez, E. Gutiérrez-Puebla, A. Monge, I. Alkorta, J. Elguero and T. Torres, *Chem. – Eur. J.*, 2008, **14**, 1342.
42 J. S. Castrucci, M. G. Helander, G. E. Morse, Z. H. Lu, C. M. Yip and T. P. Bender, *Cryst. Growth Des.*, 2012, **12**, 1095.
43 G. Zango, T. Sakurai, B. Urones, H. Saeki, W. Matsuda, M. V. Martinez-Diaz, S. Seki and T. Torres, *Chem. – Eur. J.*, 2018, **24**, 8331.
44 Y. Shu, J. Wang, Y. Tian, X. Liang, S. Lin and B. Ma, *Adv. Mater. Interfaces*, 2016, **3**, 1600179.
45 H. Geng, L. Zhu, Y. Yi, D. Zhu and Z. Shuai, *Chem. Mater.*, 2019, **31**, 6424.
46 H. Geng, X. Zheng, Z. Shuai, L. Zhu and Y. Yi, *Adv. Mater.*, 2015, **27**, 1443.
47 L. Zhu, Y. Yi, Y. Li, E. G. Kim, V. Coropceanu and J. L. Brédas, *J. Am. Chem. Soc.*, 2012, **134**, 2340.
48 C. Zhang, Y. Guo, D. He, J. Komiya, G. Watanabe, T. Ogaki, C. Wang, A. Nihonyanagi, H. Inuzuka, H. Gong, Y. Yi, K. Takimiya, D. Hashizume and D. Miyajima, *Angew. Chem., Int. Ed.*, 2021, **60**, 3261.
49 G. Zango, M. Krug, S. Krishna, V. Marinas, T. Clark, M. V. Martinez-Diaz, D. M. Guldi and T. Torres, *Chem. Sci.*, 2020, **11**, 3448.
50 J. Gotfredsen, T. Holmstrom, A. V. Munoz, F. E. Storm, C. G. Tortzen, A. Kadziola, K. V. Mikkelsen, O. Hammerich and M. B. Nielsen, *Org. Lett.*, 2018, **20**, 5821.
51 H. M. Rhoda, M. P. Kayser, Y. Wang, A. Y. Nazarenko, R. V. Belosludov, P. Kiprof, D. A. Blank and V. N. Nemykin, *Inorg. Chem.*, 2016, **55**, 9549.
52 J. Guilleme, D. Gonzlez-Rodrguez and T. Torres, *Angew. Chem., Int. Ed.*, 2011, **50**, 3506.
53 M. A. Spackman and D. Jayatilaka, *CrystEngComm*, 2009, **11**, 19.
54 J. H. Dou, Z. A. Yu, J. Zhang, Y. Q. Zheng, Z. F. Yao, Z. Tu, X. Wang, S. Huang, C. Liu, J. Sun, Y. Yi, X. Cao, Y. Gao, J. Y. Wang and J. Pei, *J. Am. Chem. Soc.*, 2019, **141**, 6561.
55 M. Schwarze, W. Tress, B. Beyer, F. Gao, R. Scholz, C. Poelking, K. Ortstein, A. A. Günther, D. Kasemann, D. Andrienko and K. Leo, *Science*, 2016, **352**, 1446.
56 K. Ortstein, S. Hutsch, M. Hambsch, K. Tvingstedt, B. Wegner, J. Benduhn, J. Kublitski, M. Schwarze, S. Schellhammer, F. Talnack, A. Vogt, P. Bäuerle, N. Koch, S. C. B. Mannsfeld, H. Kleemann, F. Ortmann and K. Leo, *Nat. Mater.*, 2021, **20**, 1407.
57 C. F. Macrae, P. R. Edgington, P. McCabe, E. Pidcock, G. P. Shields, R. Taylor, M. Towler and J. Streek, *J. Appl. Crystallogr.*, 2006, **39**, 453.

